*J. Fluid Mech.* (1969), *vol.* 38, *part* 2, *pp.* 335–352
*Printed in Great Britain*



# Magnetohydrodynamic flow between rotating coaxial disks

By C. J. STEPHENSON†
University Engineering Department, Cambridge

(Received 7 December 1968)

This is a study of the magnetohydrodynamic flow of an incompressible viscous fluid between coaxial disks, with a uniform axial magnetic field $B$. The fluid has density $\rho$, viscosity $\eta$ and electrical conductivity $\sigma$. The flow is assumed to be steady, and to be similar in the sense that the radial and tangential components of velocity increase linearly with radial distance from the axis of rotation. Most of the work is concerned with disks which are electrical insulators, one of which rotates while the other remains stationary. The imposed conditions can then be represented by the Reynolds number $R = \rho\Omega_a d^2/\eta$ and the Hartmann number $M^2 = \sigma B^2 d^2/\eta$, where $\Omega_a$ is the angular velocity of the rotating disk and $d$ is the gap between the disks. Asymptotic solutions are given for $R \ll M^2$, and numerical solutions are obtained for values of $R$ and $M^2$ up to 512. Experimental measurements are presented which are in general agreement with the theoretical flows, and the results for small values of the Hartmann number provide the first known experimental support for the purely hydrodynamic solutions in the range $100 < R < 800$.

## 1. Introduction

The steady flow of an incompressible viscous fluid between two infinite coaxial disks presents one of the few situations for which exact solutions of the Navier–Stokes equations have been obtained. Hydrodynamically, it is a two-parameter problem, with given conditions represented by (*a*) the ratio of the speeds of rotation of the disks (which may rotate in the same or the opposite sense, or one may be at rest), together with (*b*) the Reynolds number $R$, based on the gap between the disks (see equation (2.35)). Primary and secondary flows are set up in three dimensions, and the assumption is made that the flow is similar, in the sense that $v_r = r \times$ function of $z$ and $v_\theta = r \times$ function of $z$.

The topic was first discussed by Batchelor (1951), who generalized the outward-flowing boundary-layer solution of von Kármán (1921) and the inward-flowing solution of Bödewadt (1940), for single disks, and speculated on how they could be matched for the flow between two disks. The problem was pursued by Stewartson (1953), and subsequently numerical solutions were obtained by Lance & Rogers (1962), by Pearson (1965), and by Mellor, Chapple & Stokes (1968), who also made measurements of the flow for small values of the Reynolds

† Present address: IBM Research Center, Yorktown Heights, N.Y.

number ($R \leqslant 150$). Other experiments have been done for large Reynolds numbers ($R > 800$) by Picha & Eckert (1958) and by Maxworthy (private communication). A review of some of this work has been presented by Rott & Lewellen (1966).

For the case when one disk is at rest the main results may be summarized as follows. (i) For large values of the Reynolds number there are exact solutions which give an outward-flowing layer on the rotating disk and an inward-flowing layer on the stationary disk, separated by a layer containing uniform rotation and uniform axial flow. These solutions may be constructed by matching two boundary-layer solutions for single disks. The speed of rotation in the central region is approximately $0{\cdot}31\Omega_a$, where $\Omega_a$ is the speed of rotation of the spinning disk. (ii) For smaller values of $R$ ($< 300$ approximately) the numerical results show a continuous and sometimes complicated variation of velocity between the disks; these solutions cannot, therefore, be built up from two boundary layers.

The present paper is concerned with the extension of this problem to the magnetohydrodynamic case, in which the fluid is an electrical conductor, and there is a uniform imposed axial magnetic field $B$. The disks may also be electrical conductors (and make electrical contact with the fluid). It now becomes necessary to specify three more parameters, in addition to ($a$) and ($b$) above, which may be ($c$) the Hartmann number $M^2$ (see equation (2.36)), ($d$) a conductance parameter for the lower disk, and ($e$) a conductance parameter for the upper disk (see equations (2.30) and (2.32)).

The effects of the magnetic field will be complicated. Non-uniformity of angular velocity will set up radial currents $j_r$ which will produce a tangential body force $-Bj_r$. This will modify the distribution of angular velocity, and hence indirectly the secondary flow. Similarly radial motion will induce currents $-j_\theta$, and an opposing body force $-Bj_\theta$.

This paper is concerned with similarity solutions for this problem. Unfortunately the solutions cannot now be exact, owing to an induced magnetic field which increases with radius. It turns out, however, that there can be an appreciable region around the axis of rotation where the induced field is negligible, and similarity flow can therefore be obtained. (For a proof of this, see Stephenson 1967, chapter 3).

Previous work on the topic will be discussed in § 3, after derivation of the equations of motion.

## 2. Formulation of the problem

Consider the situation depicted in figure 1. A uniform incompressible fluid, having density $\rho$, viscosity $\eta$ and electrical conductivity $\sigma$, is bounded at $z = 0$ and $z = d$ by two large disks of radius $a$ ,which are uniform in $r$ and $\theta$ and have thickness $t_a$ and $t_b$ and conductivity $\sigma_a(z)$ and $\sigma_b(z)$. The disks make contact with the fluid between them, but are electrically isolated from the environment. They rotate with angular velocities $\Omega_a$ and $\Omega_b$. (We impose the condition that $|\Omega_b| \leqslant \Omega_a$.) There is a uniform imposed axial magnetic field $B$.

With the usual MHD approximations, and the assumption of steady flow, the governing equations are:

$$\rho(\mathbf{v}.\nabla)\,\mathbf{v} = -\operatorname{grad} p + \eta\nabla^2\mathbf{v} + \mathbf{j}\times\mathbf{B}, \tag{2.1}$$

$$\operatorname{div}\mathbf{v} = 0, \tag{2.2}$$

$$\operatorname{div}\mathbf{B} = 0, \tag{2.3}$$

$$\operatorname{curl}\mathbf{B} = \mu\sigma(\mathbf{E}+\mathbf{v}\times\mathbf{B}), \tag{2.4}$$

$$\operatorname{curl}\mathbf{E} = 0. \tag{2.5}$$

(See, for example, Shercliff 1965, p. 24.) It is also convenient to write

$$\mathbf{j} = (1/\mu)\operatorname{curl}\mathbf{B} = \sigma(\mathbf{E}+\mathbf{v}\times\mathbf{B}), \tag{2.6}$$

and consequently:

$$\operatorname{div}\mathbf{j} = 0. \tag{2.7}$$

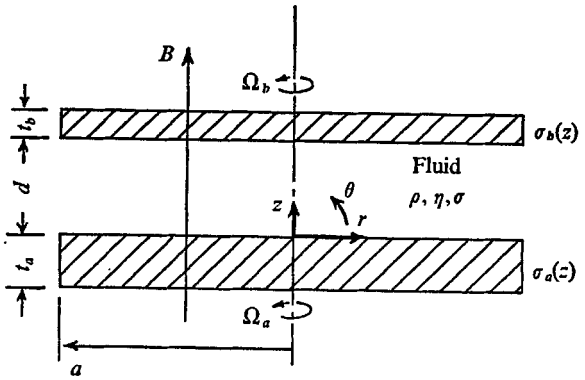


FIGURE 1. Physical model and co-ordinates.

Imposing axial symmetry, and using $\operatorname{curl}\mathbf{E} = 0$, we get

$$E_\theta = 0 \text{ everywhere.} \tag{2.8}$$

We assume that the induced field $b \ll B$ (requiring essentially that the magnetic Reynolds number based on radius $a$ should be small: see Stephenson 1967). Then $\mathbf{B} = \hat{\mathbf{z}}B$, and

$$j_\theta = -\sigma B v_r, \tag{2.9}$$

$$j_z = \sigma E_z. \tag{2.10}$$

Finally, we make the similarity substitutions:

$$v_r = r \times \text{function of } z, \tag{2.11}$$

$$v_\theta = r \times \text{function of } z; \tag{2.12}$$

whence, using $\operatorname{div}\mathbf{v} = 0$, we get

$$v_z = \text{function of } z. \tag{2.13}$$

It is now possible to derive the equations of motion without making any additional assumptions.

Using the substitutions above, the tangential equation of motion may be written:

$$\frac{\eta}{r}\frac{\partial^2}{\partial z^2}v_\theta - \rho\left\{\frac{2}{r^2}v_r v_\theta + \frac{v_z}{r}\frac{\partial}{\partial z}v_\theta\right\} = \frac{Bj_r}{r}. \tag{2.14}$$

The terms on the left-hand side of this equation are all functions of $z$ only, and therefore, using (2.6):

$$j_r = \sigma(E_r - Bv_\theta) = r \times \text{function of } z. \tag{2.15}$$

Using $\operatorname{div}\mathbf{j} = 0$ we get:

$$\frac{\partial}{\partial z}j_z = -\frac{1}{r}\frac{\partial}{\partial r}(rj_r) = \text{function of } z, \tag{2.16}$$

whence

$$j_z = \sigma E_z = \text{function of } r + \text{function of } z. \tag{2.17}$$

This holds for any value of $z$ which lies in a conducting medium, whether the medium be the fluid or a conducting disk.

Now consider a surface where a conducting medium adjoins a non-conducting medium. Such surfaces exist (*a*) between the conducting fluid and an insulating disk (if present), and (*b*) between a conducting disk (if present) and the environment (at $z = -t_a$ or $z = d + t_b$). It can be seen that there will always be at least one surface of this kind. (In fact there are always two.) At such a surface we have $j_z = 0$, and therefore in the conducting medium

$$j_z = \sigma E_z = \text{function of } z. \tag{2.18}$$

From $\operatorname{curl}\mathbf{E} = 0$ we obtain

$$\frac{\partial}{\partial r}E_z = \frac{\partial}{\partial z}E_r, \tag{2.19}$$

$$E_r = \text{function of } r. \tag{2.20}$$

Hence, with (2.15),

$$E_r = r \times \text{const}. \tag{2.21}$$

By similarly considering any other surface which may exist between this medium and another conducting medium, it can be shown that these relationships hold throughout all conducting media which may be present. The following relationships are therefore general, wherever $\sigma > 0$.

$$E_r = r \times \text{const} = (\text{say}) - \chi B\Omega_a r, \tag{2.22}$$

$$E_\theta = 0, \tag{2.23}$$

$$E_z = \text{function of } z, \tag{2.24}$$

$$j_r = \sigma B(v_\theta - \chi\Omega_a r), \tag{2.25}$$

$$j_\theta = -\sigma B v_r, \tag{2.26}$$

$$j_z = \sigma E_z = \text{function of } z. \tag{2.27}$$

Integrating (2.25) between $z = -t_a$ and $z = d + t_b$, and putting

$$\int_{-t_a}^{d+t_b} j_r\,dz = 0,$$

we get

$$\chi = \int_{-t_a}^{d+t_b} \sigma(z)\,v_\theta\,dz \Big/ r\Omega_a \int_{-t_a}^{d+t_b} \sigma(z)\,dz. \tag{2.28}$$

This dimensionless quantity $\chi$ denotes the strength of the induced radial electric field $E_r$. It is proportional to the average angular velocity of the disks and fluid, weighted according to their thickness and conductivity. Now let

$$s = \int_{-t_a}^{d+t_b} \sigma(z)\,dz, \tag{2.29}$$

and define dimensionless parameters of conductivity:

$$S_a = \frac{1}{s}\int_{-t_a}^{0} \sigma_a(z)\,dz \quad \text{(lower disk)}, \tag{2.30}$$

$$S_f = \frac{\sigma d}{s} \quad \text{(fluid)}, \tag{2.31}$$

$$S_b = \frac{1}{s}\int_{d}^{d+t_b} \sigma_b(z)\,dz \quad \text{(upper disk)}; \tag{2.32}$$

then from (2.28) it can be shown that

$$\chi = \frac{S_a\Omega_a + S_f\omega_{av} + S_b\Omega_b}{\Omega_a}, \tag{2.33}$$

where $\omega_{av}$ is the average angular velocity of the fluid.

Finally we define dimensionless parameters:

$$\zeta = z/d, \tag{2.34}$$

$$R = \rho\Omega_a d^2/\eta = \text{Reynolds number based on gap between disks}, \tag{2.35}$$

$$M^2 = \sigma B^2 d^2/\eta = \text{Hartmann number}; \tag{2.36}$$

and substitute:

$$v_r = r\Omega_a F(\zeta), \quad v_\theta = r\Omega_a G(\zeta), \quad v_z = d\Omega_a H(\zeta), \tag{2.37}$$

$$p = \eta\Omega_a P(\zeta) + \tfrac{1}{2}\lambda\rho\Omega_a^2 r^2. \tag{2.38}$$

We then obtain the equations of motion in the following dimensionless form:

$$F'' = R(F^2 - G^2 + F'H + \lambda) + M^2 F, \tag{2.39}$$

$$G'' = R(2FG + G'H) + M^2(G - \chi), \tag{2.40}$$

$$H' + 2F = 0, \tag{2.41}$$

$$Q' = G; \tag{2.42}$$

with boundary conditions:

$$F = H = Q = 0, \quad G = 1 \quad \text{at} \quad \zeta = 0, \tag{2.43}$$

$$F = H = 0, \quad G = \frac{\Omega_b}{\Omega_a}, \quad Q = \frac{\chi - S_a - S_b(\Omega_b/\Omega_a)}{S_f} \quad \text{at} \quad \zeta = 1. \tag{2.44}$$

Here dashes signify differentiation with respect to $\zeta$, and the variable $Q(\zeta)$ has been introduced in order to incorporate the final boundary condition. The pressure term $P(\zeta)$ is given by:

$$P = -2F - \tfrac{1}{2}RH^2 + (\text{say})\,\Pi. \tag{2.45}$$

If the equations remained valid to the edge of the disks at $r = a$, the torque on (say) the lower disk would be:

$$T_a = \tfrac{1}{2}\pi\,\Omega_a a^4\{(\eta/d)\,G'(0) - (1-\chi)\,B^2 s S_a\}. \tag{2.46}$$

Before attempting to relate these equations to a real flow, we shall examine the assumptions which have been made in deriving them. It will, however, be convenient to postpone this until § 6, after the solutions have been presented.

## 3. Previous work

The magnetohydrodynamic flow between two disks was analyzed by Srivistava & Sharma (1961), who imposed the condition that one disk be stationary and that the Reynolds number $R \ll$ the Hartmann number $M^2$. They obtained formal expansions for $F$, $G$, $H$ and $\lambda$ in powers of $R$, evaluated the first terms, and examined the torque on the stationary disk. Unfortunately they omitted the term $M^2\chi$ from (2.40), with the results (i) that their expansions are valid only if the stationary disk is a perfect conductor, or has infinite thickness (and is not an insulator), and (ii) that their expression for the torque is completely erroneous.

Several writers have examined the magnetohydrodynamic flow over a single disk. Rizvi (1962) looked at this problem with a weak magnetic field. Unfortunately he supposed the disk to be a perfect conductor, which yields an indeterminate radial electric field, and the boundary conditions he gives are incompatible with his equations. Sparrow & Cess (1962) studied the case of an insulating disk rotating in fluid which has no angular velocity at large axial distances from the disk, and they obtained the solution by numerical integration. Kakutani (1962) solved the identical problem by joining two expansions.

Finally, King & Lewellen (1964) analyzed the behaviour of rotating fluid over a stationary surface, with and without an axial magnetic field. They obtained results by means of numerical integration, for $v_\theta \propto r^n$, where $-1 \leqslant n \leqslant 1$. They found that the magnetic field tends to reduce radial flow and damp out variations in angular velocity.

## 4. Asymptotic solutions for $R \ll M^2$

The equations (2.39)–(2.42) may be rewritten as

$$\frac{R}{M^2}(F^2 - G^2 + F'H + \lambda) - \frac{F''}{M^2} + F = 0, \tag{4.1}$$

$$\frac{R}{M^2}(2FG + G'H) - \frac{G''}{M^2} + (G - \chi) = 0, \tag{4.2}$$

$$H' + 2F = 0, \tag{4.3}$$

$$Q' - G = 0. \tag{4.4}$$

If we consider the case of $R \ll M^2$, and substitute $N = M^2/R$, the unknown quantities may be formally expanded in powers of $1/N$, as follows:

$$F(\zeta) = f_0(\zeta) + \frac{1}{N} f_1(\zeta) + \frac{1}{N^2} f_2(\zeta) + \ldots, \tag{4.5}$$

$$G(\zeta) = g_0(\zeta) + \frac{1}{N} g_1(\zeta) + \frac{1}{N^2} g_2(\zeta) + \ldots, \tag{4.6}$$

$$H(\zeta) = h_0(\zeta) + \frac{1}{N} h_1(\zeta) + \frac{1}{N^2} h_2(\zeta) + \ldots, \tag{4.7}$$

$$Q(\zeta) = q_0(\zeta) + \frac{1}{N} q_1(\zeta) + \frac{1}{N^2} q_2(\zeta) + \ldots, \tag{4.8}$$

$$\lambda = \lambda_0 + \frac{1}{N} \lambda_1 + \frac{1}{N^2} \lambda_2 + \ldots, \tag{4.9}$$

$$\chi = \chi_0 + \frac{1}{N} \chi_1 + \frac{1}{N^2} \chi_2 + \ldots, \tag{4.10}$$

Substituting these into (4.1)–(4.4) and equating terms of order $1/N^0$, $1/N$ we get the first two sets of equations as follows.

$$-\frac{f_0''}{M^2} + f_0 = 0, \tag{4.11}$$

$$-\frac{g_0''}{M^2} + g_0 - \chi_0 = 0, \tag{4.12}$$

$$h_0' + 2f_0 = 0, \tag{4.13}$$

$$q_0' - g_0 = 0; \tag{4.14}$$

with boundary conditions:

$$f_0 = h_0 = q_0 = 0, \quad g_0 = 1 \quad \text{at} \quad \zeta = 0, \tag{4.15}$$

$$f_0 = h_0 = 0, \quad g_0 = \frac{\Omega_b}{\Omega_a}, \quad q_0 = \frac{\chi_0 - S_a - S_b(\Omega_b/\Omega_a)}{S_f} \quad \text{at} \quad \zeta = 1. \tag{4.16}$$

Also

$$f_0^2 - g_0^2 + f_0' h_0 + \lambda_0 - \frac{f_1''}{M^2} + f_1 = 0, \tag{4.17}$$

$$2f_0 g_0 + g_0' h_0 - \frac{g_1''}{M^2} + (g_1 - \chi_1) = 0, \tag{4.18}$$

$$h_1' + 2f_1 = 0, \tag{4.19}$$

$$q_1' - g_1 = 0; \tag{4.20}$$

with boundary conditions:

$$f_1 = g_1 = h_1 = q_1 = 0 \quad \text{at} \quad \zeta = 0, \tag{4.21}$$

$$f_1 = g_1 = h_1 = 0, \quad q_1 = \chi_1/S_f \quad \text{at} \quad \zeta = 1 \tag{4.22}$$

It is easy to show that

$$f_0 = h_0 = g_1 = q_1 = 0 \quad \text{everywhere}; \tag{4.23}$$

and the equations (4.12) and (4.14) yield the solution

$$\chi_0 = \frac{(\mathscr{C} - 1) S_f \{1 + (\Omega_b/\Omega_a)\} + M\mathscr{S}\{S_a + S_b(\Omega_b/\Omega_a)\}}{2(\mathscr{C} - 1) S_f + M\mathscr{S}(S_a + S_b)}, \tag{4.24}$$

$$g_0(\zeta) = \chi_0 + \frac{(\Omega_b/\Omega_a) - \chi_0 - (1 - \chi_0)\mathscr{C}}{\mathscr{S}} \sinh M\zeta + (1 - \chi_0) \cosh M\zeta, \tag{4.25}$$

where $\mathscr{S} = \sinh M$ and $\mathscr{C} = \cosh M$. Equation (4.25) may be recognized as that governing Hartmann flow between two parallel plane surfaces possessing a steady relative velocity in their own plane. The effects of rotation have, therefore, not yet appeared.

The next non-zero terms are $\lambda_0, f_1$ and $h_1$, which can be obtained from (4.17) and (4.19). The explicit solution is, however, complicated, and will not be given here. Instead, profiles of $g_0(\zeta)$ and $f_1(\zeta)$ are shown in figure 2, for the case when both disks are insulators, and one of them is at rest (i.e. $S_a = S_b = \Omega_b = 0$).

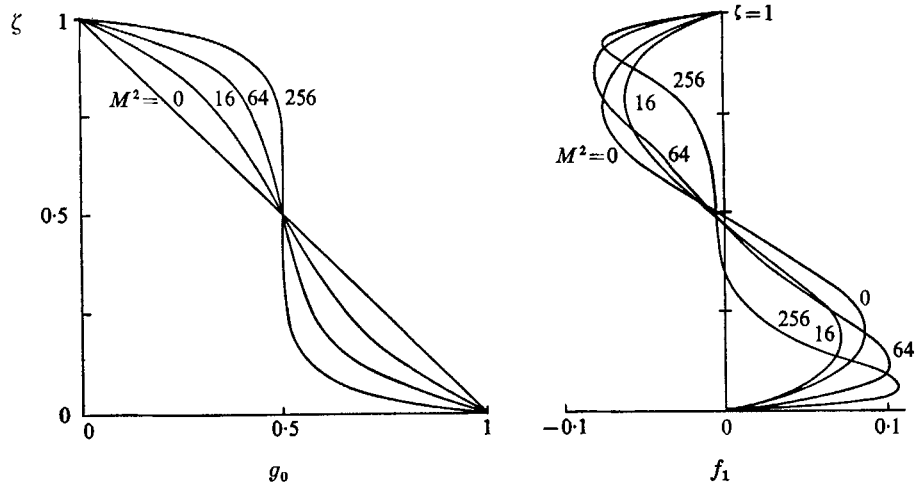


FIGURE 2. Profiles of tangential and radial velocities for $R \ll M^2 + 25$.

These same solutions hold for the case of $R \ll 1$, whatever the value of $M$. (This can be shown by replacing (4.5)–(4.10) by expansions in powers of $R$, and using (2.39) and (2.40) in place of (4.1) and (4.2): cf. Srivistava & Sharma 1961.) Thus the solution for $M = 0$ is the limit of the hydrodynamic solutions as $R \to 0$. In fact, the validity of these asymptotic solutions seems to extend much further still, and comparison with the numerical results described in the next section of this paper indicates that they lie close to the exact solutions provided only that $R \ll M^2 + 25$. (This is an approximate limitation, obtained empirically.)

Other points relating to the results are as follows. (*a*) As $M$ increases the central layer tends towards uniform rotation; also the radial flow decreases, and what remains of it becomes concentrated in boundary layers of thickness $\delta \propto 1/M$. (*b*) The profiles for $f_1$ show distinctly different shapes for the inward and outward flowing layers. It is this which accounts for the slight inward drift which appears in the central layers. (*c*) For $M = 0$, it can be shown that $\lambda_0 = 0{\cdot}3$, which agrees with the value of $\lambda$ obtained from solutions of the hydrodynamic problem for $R \to 0$; and for $M \to \infty$, it can be shown that $\lambda_0 = 0{\cdot}25$, which corresponds to solid body rotation, with $G = 0{\cdot}5$.

## 5. Numerical solutions

From now on in this paper we shall be concerned only with insulating disks, one of which is stationary, i.e. $S_a = S_b = \Omega_b = 0$. (These are the same conditions as those applying to the profiles of figure 2.) In this case

$$\chi = \int_0^1 G(\zeta)\, d\zeta = \frac{\textit{average angular velocity of fluid}}{\Omega_a} = (\text{say})\, G_{av}. \tag{5.1}$$

(It turns out that this is a useful quantity for making comparisons with experimental measurements: see § 7.) It is necessary to use numerical methods to obtain solutions for the general case, with arbitrary values of $R$ and $M^2$. The method which was used will be briefly described.

The equations (2.39)–(2.42) are rewritten as six first-order differential equations, and integrated by the fourth-order Runge–Kutta process, with rounding error correction. The integration is done in two parts, starting at the inner surface of each disk and meeting at an intermediate point in the fluid, so as to avoid integrating 'backwards' through either boundary layer. To start the integration from $\zeta = 0$ it is necessary to have estimates for $f'(0)$, $g'(0)$, $\lambda$ and $\chi$; and to start from $\zeta = 1$ it is necessary to have estimates for $f'(1)$, $g'(1)$, $\lambda$ and $\chi$. Unless these six estimates are all correct, there will in general be six matching errors where the integrations meet.

Each of the six estimates, or 'starting values', is incremented in turn, and the corresponding changes in matching errors are obtained as a $6 \times 6$ matrix. Linear relationships are assumed between the matching errors and the starting values; on this basis the starting values are adjusted so as to eliminate the errors, and the integration is repeated. In practice some errors usually remain, and the cycle is continued until they have been reduced to an acceptable level.

Unfortunately this process of 'convergence' towards the solution will in general succeed only if the estimates are all fairly accurate. In this problem it was found that initial errors in the estimates of about 1 part in $10^4$ could (in some cases) cause the process to *diverge*, away from the correct solution. A method was therefore developed for building up a series of solutions, for increasing (or decreasing) values of $R$ or $M^2$, so that estimates for the starting values could be obtained automatically by extrapolation from the previous few solutions in the series. If at any stage the extrapolated estimates were not good enough to yield convergence, one or more intermediate solutions were obtained, between the last one found and the one now required, so that the estimates could be improved.

This method worked well, and a network of solutions was obtained for $1 \leqslant R \leqslant 512$, $0 \leqslant M^2 \leqslant 512$. In principle, all the solutions could be built up from any one given set of starting values, which could, for example, be obtained from one of the asymptotic solutions of the last section. In fact, the solutions were initiated from several different points, using data for the hydrodynamic problem which were deposited by Lance & Rogers (1962) at the Royal Society.

A summary of the results is presented in figures 3–6. The first three of these give profiles of $F(\zeta)$ and $G(\zeta)$ for three values of the Reynolds number $R$ and various values of the Hartmann number $M^2$. It can be seen that the main effect

of a weak field is to iron out variations in the main body of the fluid; and that a strong field (for which $M^2 > R$) produces a substantial reduction in the radial flow. As $R$ or $M^2$ increase above about 300, a layer of uniform rotation appears in the main body of the fluid, and radial velocities become confined to the

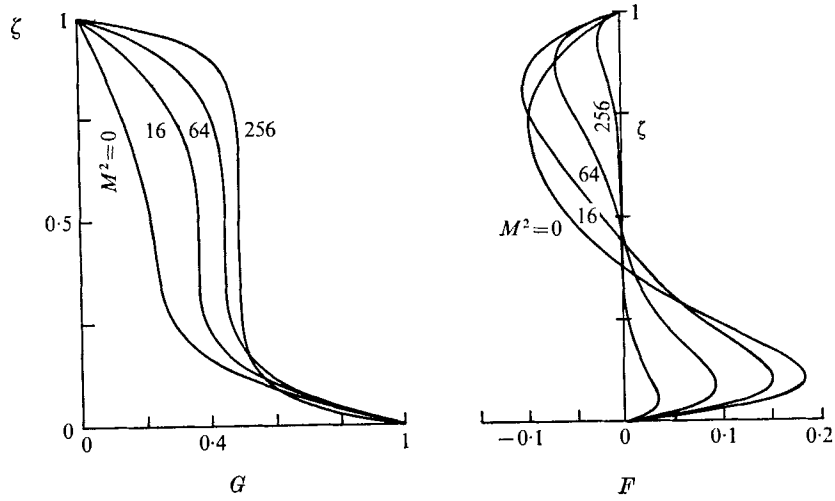


FIGURE 3. Profiles of tangential and radial velocities for $R = 83$.

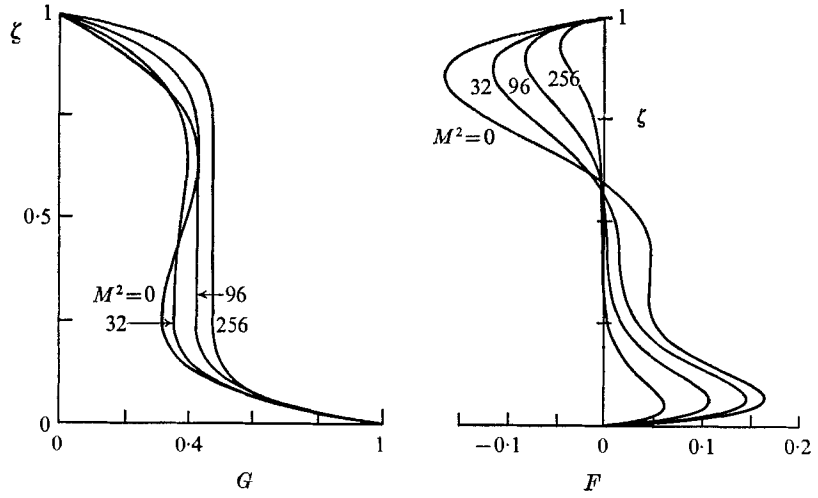


FIGURE 4. Profiles of tangential and radial velocities for $R = 176$.

boundary layers. In the limit, for large values of $R$ or $M^2$, the velocity profiles could be constructed from the appropriate boundary layer solutions, and would yield boundary layers for which the thickness

$$\delta \propto 1/R^{\frac{1}{2}} \quad \text{for} \quad R \gg M^2, \tag{5.2}$$

or

$$\delta \propto 1/M \quad \text{for} \quad M^2 \gg R. \tag{5.3}$$

Figure 6 shows the variation of $\chi$ (or $G_{av}$) with $\sqrt{R}$ for various values of $M^2$. For $R/M^2 \to 0$, it can be seen that $\chi \to 0{\cdot}5$, which is in agreement with the asymptotic solutions of the last section; and for $R/M^2 \to \infty$, it can be shown that $\chi \to 0{\cdot}31$ approximately. For $M = 0$, $\chi$ passes through a minimum of 0·2615 at $R \approx 83$ and a maximum of 0·3741 at $R \approx 671$. This is the reason why profiles are shown for these particular values of $R$.

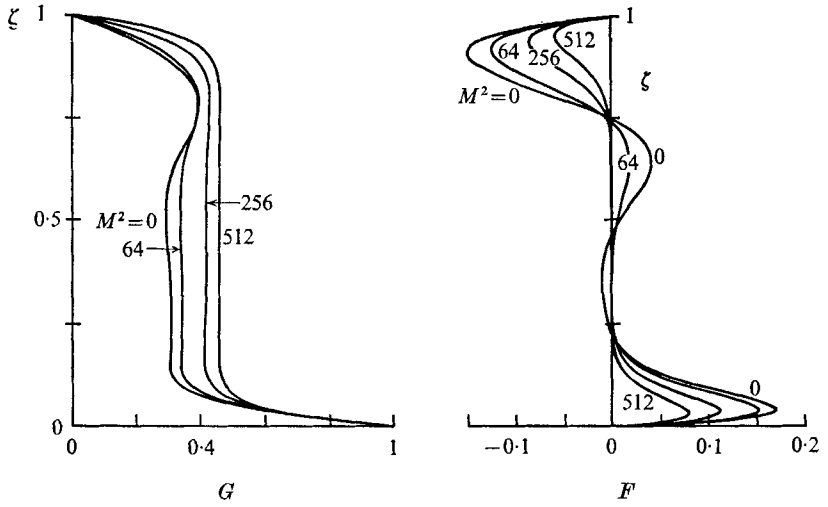


FIGURE 5. Profiles of tangential and radial velocities for $R = 512$.

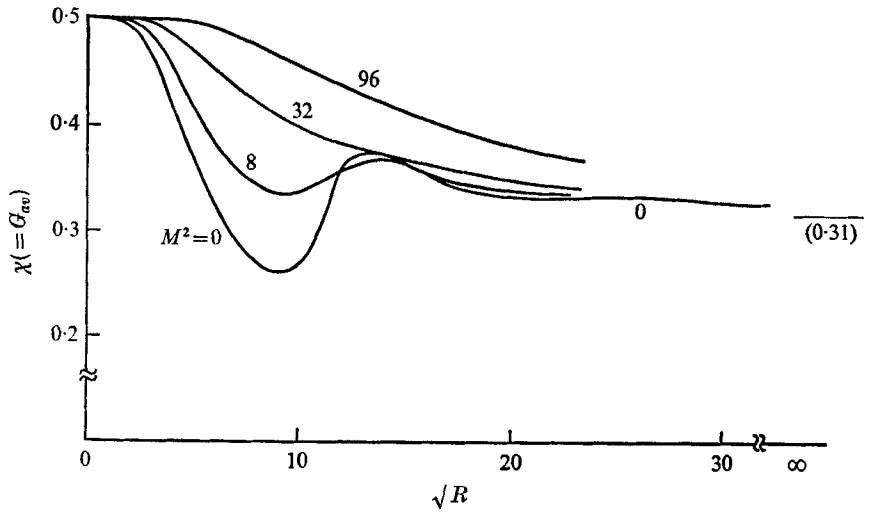


FIGURE 6. $\chi$ (or $G_{av}$) *versus* $\sqrt{R}$.

## 6. Realization of similarity flow

In this section we consider in more detail some of the assumptions which were made in § 2, and we discuss the practical difficulties is realizing the similarity solutions which have been presented.

### 6.1. *Possibility of non-similarity solutions*

In the case of the flow over a single disk, dimensional arguments can be used to show that the only possible steady solutions are similarity solutions (in which $v_r = r \times$ function of $z$ and $v_\theta = r \times$ function of $z$). These arguments cannot be applied to the flow between two disks owing to the existence of the scale length $d$, and it is in principle possible for there to be steady solutions in which the velocity varies in a complicated way with $r$, $\theta$ and $z$. It is not known whether such solutions exist, or (if they do) whether they are stable.

### 6.2. *Other kinds of similarity solution*

It is known from Mellor *et al.* (1968), and from other work by the present writer, that at least one of the solutions presented in the last section is not unique. For $R = 512$, $M = 0$, other similarity solutions exist in which some of the fluid rotates in the opposite sense to the spinning disk. It seems almost certain that this kind of flow could be established in practice only if the conditions at the edge of the disks particularly favoured it (see below).

### 6.3. *Edge effects*

It has sometimes been assumed that the conditions at the edge of the disks will have a negligible effect on the flow near the axis provided that the ratio $a/d$ is sufficiently large. Yet according to the similarity assumptions, $v_r$ and $v_\theta$ are proportional to $r$, so that any defects in radial or tangential momentum due to the geometry at the edge will increase indefinitely with $a$. Nevertheless, the assumption seems to be reasonable for an outward-flowing layer, since the outward motion is set up by centrifugal forces, and will at any radius be dominated by events at smaller radii. But the initiation of inward flow is more complicated: it must occur somewhere near the edge of the disks, and there may be conditions in which it depends crucially on the conditions in this region.

It would be possible, for theoretical argument, to suppose that a system of pumps and ducts was set up around the edge of the disks, and was adjusted to give the flow required by the appropriate solution at the radius $a$. Then provided that the solution was stable, it should be possible to sustain the flow between the disks. It is, however, more realistic to consider (i) disks surrounded with a fixed cylindrical shroud, or (ii) unshrouded disks immersed in a stationary fluid. The following points apply to these situations.

(*a*) In the similarity solutions (of the kind considered here) the main body of fluid possesses an axial velocity towards the rotating disk. In the presence of a shroud, however, there must be (owing to continuity) an extensive region around the edge of the disks where the axial flow is reversed, and where similarity flow cannot therefore occur. Similarly it is possible to show that for $M \neq 0$ there is an axial current which must also be reversed around the edge of the disks.

(*b*) In the similarity solutions (of the kind considered here) there are appreciable tangential velocities in the inward-flowing boundary layer. Consider the origin of these velocities, first when there is no magnetic field ($M = 0$). There is little difficulty in the presence of a shroud, for the fluid around the edge will

have been supplied from the outward-flowing layer and will already possess tangential momentum. (See Rogers & Lance (1964) on the growth of an inward-flowing layer on a stationary disk.) But in the absence of a shroud it is not clear how these tangential velocities could be set up. In fact the reported experiments indicate that an approach to similarity flow (of the kind considered here) is obtained in practice only if there is a shroud; otherwise the bulk of the fluid remains almost stationary and an inward-flowing boundary layer does not develop (see Stewartson 1953; Picha & Eckert 1958). A magnetic field is likely to alleviate this problem, for it provides a body force which can be the source of tangential velocities well away from the rotating disk.

(*c*) For $M = 0$, and in the absence of viscosity, the Raleigh criterion for radial instability is that

$$0 > \frac{\partial}{\partial r}(rv_\theta).$$

There are bound to be regions around the edge of the disks where this condition will be fulfilled and where (therefore) steady flow is unlikely to be supported. (This problem could be overcome by using a rotating shroud. This was tried by Maxworthy (private communication) but it apparently produced some singular effects at $r \to 0$.)

These edge effects are complicated, and are not amenable to easy analysis. In practice it seems best to use a stationary shroud, and to set $a/d$ reasonably large (but see below).

### 6.4. *Stability and turbulence*

In the equations governing similarity flow (namely (2.39)–(2.42)), radial and tangential dependence have been specifically excluded; and it follows that, whatever method may be used to obtain solutions, it cannot provide any direct information on their stability to three-dimensional disturbances. We may note, however, that even a solution which was stable near the axis would in practice cease to remain so beyond some critical radius, owing to the onset of turbulence.

At first sight we may expect the flow to become turbulent when $R_r = \rho\Omega_a r^2/\eta$ (Reynolds number based on radius) exceeds some critical value. In an outward-flowing layer, however, the conditions at any radius will be dominated by events at smaller radii, where $R_r$ is smaller, and this will have a stabilizing effect upon the flow. Laminar flow has in fact been reported in outward-flowing layers having values of $R_r$ exceeding $3 \times 10^5$. In an inward-flowing layer, on the other hand, conditions are dominated by events at larger radii, where $R_r$ is larger, and stability may be difficult to achieve. Despite this, there have been a number of apparently successful experiments on laminar flow between two disks (reported elsewhere in the literature, and in the next section of this paper) which have had values of $R_r$ rising to over $10^5$.

## 7. Experiments

Measurements were made on the flow of mercury between insulating disks, one of which rotated while the other was held at rest. The heart of the apparatus is shown in figure 7. The disks were made of 'Tufnol', a smooth impregnated

paper laminate, and the working space between them was 10 in. in diameter. The lower disk rotated at a speed of between 0 and 12 radians/sec. A stationary shroud, also made of Tufnol, was fixed to the upper disk. For reasons of mechanical

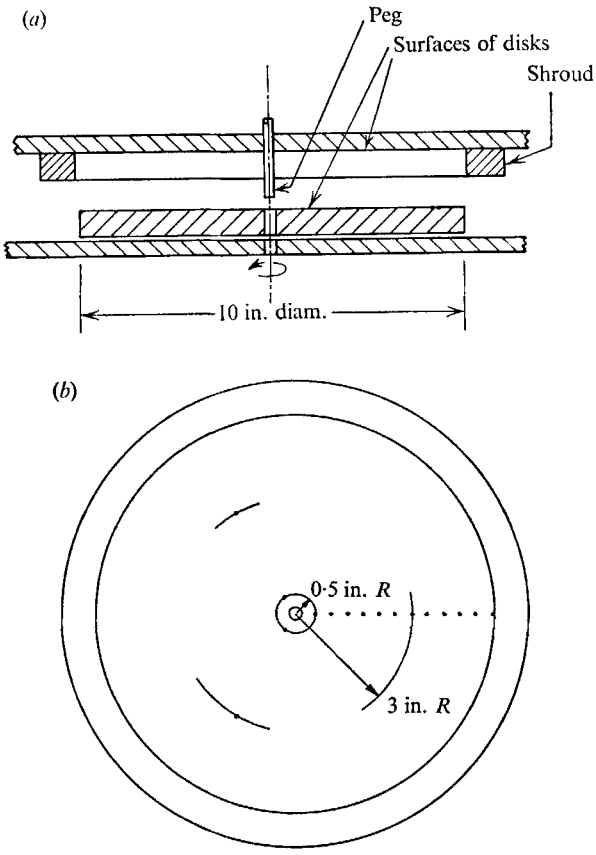


FIGURE 7. Experimental apparatus. (*a*) Elevation of disks, shown separated. (*b*) Underside view of upper disk, showing positions of probe wires.

stability there was an insulated brass peg projecting downwards from the centre of the upper disk and bearing in an axial hole in the lower disk. (The influence of this peg on the flow is likely to have been negligible, and will be ignored.) Through the upper disk there passed 14 pieces of 20 s.w.g. palladium wire, laid out as shown in figure 7 (*b*), having exposed tips flush with the surface of the disk. The space between and around the disks was filled with mercury, and the gap between the disks could be adjusted between 0 and 0·7 in.

The apparatus was mounted in a large electromagnet which produced (for these experiments) an axial field of up to 0·11 Wb/m$^2$. Sheets of armature steel, fixed behind the disks, maintained a uniform field between them. At 15 °C the physical constants for mercury in m.k.s. units are $\rho = 1{\cdot}36 \times 10^4$, $\eta = 1{\cdot}58 \times 10^{-3}$ and $\sigma = 1{\cdot}05 \times 10^6$. Thus for $d = 0{\cdot}5$ cm, $\Omega_a = 1$ rad/sec and $B = 0{\cdot}1$ Wb/m$^2$, we get $R \approx M^2 \approx 200$.

Palladium was used for the probe wires because it exhibits approximately the same thermo-electric potentials as mercury. The voltages between the probes were measured with a bridge and reflecting galvanometer. According to the theory of § 2, $E_\theta = 0$ everywhere, and the potential difference between two wires situated at radii $r_1$ and $r_2$ will be

$$V_2 - V_1 = -\int_{r_1}^{r_2} E_r dr = B\Omega_a \frac{r_2^2 - r_1^2}{2} \chi. \tag{7.1}$$

Hence

$$\chi = G_{av} = \frac{2}{B\Omega_a} \frac{V_2 - V_1}{r_2^2 - r_1^2} \tag{7.2}$$

(see equations (2.23) and (5.1)). All the quantities on the right-hand side of this equation can be set or measured, and the experimental values of $\chi$ (or $G_{av}$) obtained from here can be compared with theory.

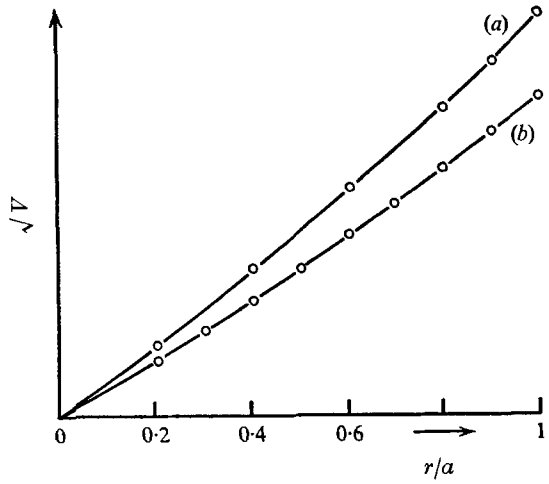


FIGURE 8. Radial dependence of electric potential. Curve (*a*): $R \sim 1000$, $M^2 \sim 100$, $a/d = 25{\cdot}4$. Curve (*b*): $R \sim 180$, $M^2 \sim 12$, $a/d = 25{\cdot}4$.

Figure 8 shows the measured dependence of $\sqrt{V}$ on radius, which is linear for true similarity flow. Two results are given, for $R \gg M^2$, which is likely to be the most difficult case. It can be seen that the slope of the curves increases slightly with radius, indicating that the mean rotation of the fluid was greater towards the edge of the disks than near the axis. There is, however, reasonable linearity within $r/a < 0{\cdot}6$. (The vertical scale on this graph is arbitrary. Also, the potentials at $r = 0$ have been estimated by extrapolation from the probe readings at $r/a = 0{\cdot}1$. These readings then cease to contain any independent information, and are omitted from the graph.)

The main results are given and compared with theory in figure 9. The full curves have been obtained from the numerical solutions, or by interpolation from them. The broken lines show approximate extensions for large values of $R$ and $M^2$, beyond the range of the numerical solutions. They are based on curves, for $R$ and $M^2 \leqslant 512$, having the same ratio of $R/M^2$. These curves are slightly modified at large values of $R$ to make approximate allowance for the

fact that $G_{av} \to 0{\cdot}31$ as $R \to \infty$ (cf. $G_{av} = 0{\cdot}3316$ at $R = 512$, $M = 0$; and $G_{av} = 0{\cdot}3279$ at $R = 1024$, $M = 0$).

The experimental points have been obtained from probe readings, using equation (7.2). In all these cases the readings were taken between the three inner

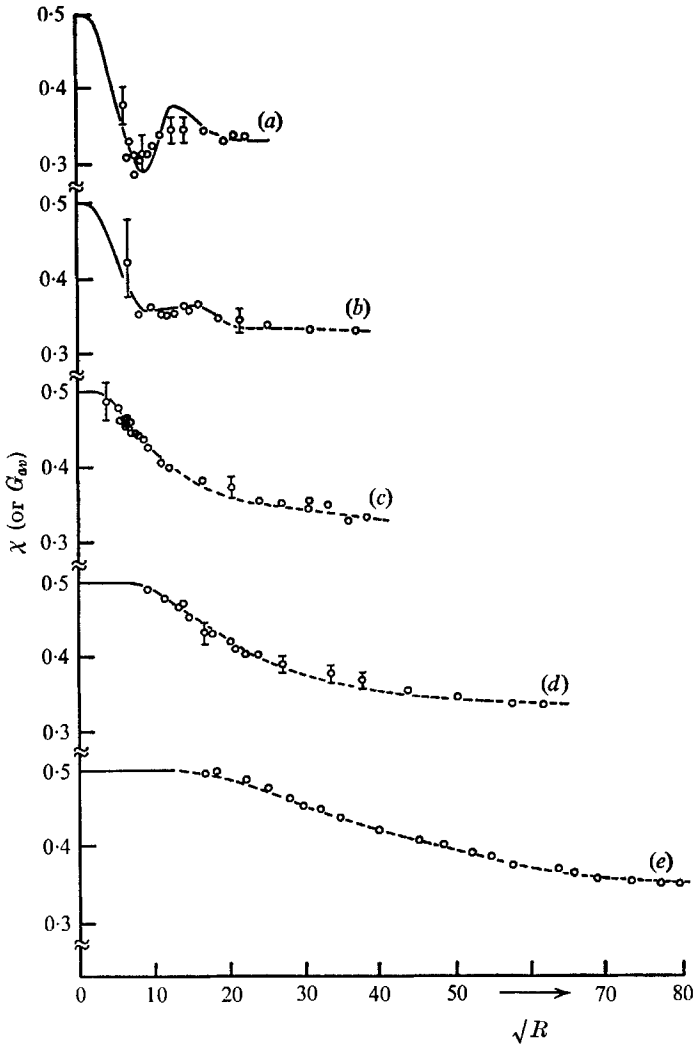


FIGURE 9. Main experimental results, compared with theory. O, experimental points; —, from numerical solutions; – – –, approximate extrapolation from numerical solutions. Curve (*a*): $M^2 \sim 1{\cdot}7$, $a/d = 25{\cdot}4$. Curve (*b*): $M^2 = 12$, $a/d = 25{\cdot}4$. Curve (*c*): $M^2 = 50$, $a/d = 25{\cdot}4$. Curve (*d*): $M^2 = 200$, $a/d = 12{\cdot}7$. Curve (*e*): $M^2 = 800$, $a/d = 12{\cdot}7$.

probes and the three probes at a radius of 3 in., which were connected *via* resistors so as to yield a mean potential difference. This gives a measure of the fluid rotation inside $r = 3$ in., i.e. inside $r/a = 0{\cdot}6$.

The probe readings were never entirely steady: they usually wandered through 1 % or 2 % of their mean values, and occasionally drifted by up to 5 %. A point on

the graph generally represents the average of between 4 and 20 actual readings, with minor corrections to allow for unavoidable drift of the magnetizing current and the speed of rotation of the lower disk. The error bars which are given may be taken to show roughly 95 % confidence limits. The greatest possible errors occur for the smaller values of $R$ and $M$, owing to the fact that the measured voltages fall to less than $2\mu$V.

It can be seen that the experimental results are in over-all agreement with the theory. There is, however, a need for caution on two points. (*a*) Significance can be attached only to the goodness of fit between the *shapes* traced out by the experimental points and the *shapes* of the theoretical curves, and *not* to the over-all *level* of the points. This is because there was no direct and accurate means of measuring the strength of the magnetic field during the experiments, and it was therefore estimated from the probe readings themselves, by finding that value which gave the best agreement between measurement and theory for large values of the Reynolds number $R$, where the measured voltages were greatest, and generally most accurate, and where the theoretical curves for $\chi$ become fairly level, approaching 0·31. (*b*) The fact that the measured and theoretical values of $\chi$ agree fairly well does not guarantee that the velocity profiles were necessarily in agreement. In the case (for example) of $R \gg M^2$ it is possible that the inward-flowing layer succeeded in transporting the right amount of fluid, and in ejecting it with the right tangential velocity, while failing to exhibit the undulating characteristics of the theoretical solutions.

It is unfortunate that there was no direct and accurate way of measuring the magnetic field during the experiments. This situation arose because at the time the apparatus was designed it was expected that the field would be a sufficiently repeatable function of the magnetizing current (which *was* measured). Subsequently, measurements on the magnet showed that this was not in fact the case. It may, however, be stated that the fields deduced from the probe readings are all compatible with the measurements of the magnetizing current.

Despite the limitations, it seems safe to conclude that, given the experimental conditions used here, there was a definite disposition in favour of the theoretical similarity flows. (In figure 9 the only significant deviation between experiment and theory occurs for $M^2 = 1{\cdot}7$, in the region of $R = 176$, where the theoretical velocity profiles display a positive tangential velocity gradient in the body of the fluid, which may be difficult to obtain in practice.) So far as is known by the writer, the results for $M^2 \leqslant 12$, which show a definite minimum and maximum in $\chi$, provide the only approach to an experimental confirmation of the purely hydrodynamic similarity solutions for values of the Reynolds number in the range $100 < R < 800$.

The author wishes to express his appreciation to Dr M. D. Cowley for numerous helpful discussions during the course of this work.

## REFERENCES


BATCHELOR, G. K. 1951 Note on a class of solutions of the Navier–Stokes equations representing steady rotationally-symmetric flow. *Quart. J. Mech. Appl. Math.* **4**, 29.

BÖDEWADT, U. T. 1940 Die Drehströmung über festem Grunde. *Z. Ang. Math. Mech.* **20**, 241.

KAKUTANI, T. 1962 Hydromagnetic flow due to a rotating disk. *J. Phys. Soc. Japan*, **17**, 1496.

KING, W. S. & LEWELLEN, W. S. 1964 Boundary layer similarity solutions for rotating flows with and without magnetic interaction. *Phys. Fluids*, **7**, 1674.

LANCE, G. N. & ROGERS, M. H. 1962 The axially asymmetric flow of a viscous fluid between two infinite rotating disks. *Proc. Roy. Soc.* A **266**, 109.

MELLOR, G. L., CHAPPLE, P. J. & STOKES, V. K. 1968 On the flow between a rotating and a stationary disk. *J. Fluid Mech.* **31**, 95.

PEARSON, C. E. 1965 Numerical solutions for the time-dependent viscous flow between two rotating coaxial disks. *J. Fluid Mech.* **21**, 623.

PICHA, K. G. & ECKERT, E. R. G. 1958 Study of the air flow between coaxial disks rotating with arbitrary velocities in an open or enclosed space. *Proc. 3rd U.S. Nat. Congr. Appl. Mech.* p. 791.

RIZVI, S. A. T. 1962 On the steady rotation of a disk in magnetohydrodynamics. *Appl. Sci. Res.* B **10**, 62.

ROGERS, M. H. & LANCE, G. N. 1964 The boundary layer on a disk of finite radius in a rotating fluid. *Quart. J. Mech. Appl. Math.* **17**, 319.

ROTT, N. & LEWELLEN, W. S. 1966 Flow between a rotating and stationary disk. *Prog. Aeron. Sci.* **7**, 136.

SHERCLIFF, J. A. 1965 *A Textbook of Magnetohydrodynamics.* Oxford: Pergamon.

SPARROW, E. M. & CESS, R. D. 1962 Magnetohydrodynamic flow and heat transfer about a rotating disk. *J. Appl. Mech.* **29**, 181.

SRIVISTAVA, A. C. & SHARMA, S. K. 1961 The effect of a transverse magnetic field on the flow between two infinite disks—one rotating and the other at rest. *Bull. Acad. Pol. Sci.* (*ser. Sci. Tech.*) **9**, 639.

STEPHENSON, C. J. 1967 Ph.D. thesis. University of Cambridge.

STEWARTSON, K. 1953 On the flow between two rotating coaxial disks. *Proc. Camb. Phil. Soc.* **49**, 533.

VON KÁRMÁN, TH. 1921 Über laminare und turbulente Reibung. *Z. Ang. Math. Mech.* **1**, 233. Translated: On laminar and turbulent friction. *NACA Tech. Memo.* no. 1092.